I&EC research
Industrial & Engineering Chemistry Research

Article

Cite This: Ind. Eng. Chem. Res. 2018, 57, 6821−6829

pubs.acs.org/IECR

Hydrogenation of CO_2 to Dimethyl Ether over Brønsted Acidic PdZn Catalysts

Hasliza Bahruji,*[,†] Robert D. Armstrong,*[,†] Jonathan Ruiz Esquius,[†] Wilm Jones,[‡] Michael Bowker,[†,‡] and Graham J. Hutchings[†]

[†]Cardiff Catalysis Institute, School of Chemistry, Cardiff University, Main Building, Park Place, CF10 3AT Cardiff, United Kingdom
[‡]The UK Catalysis Hub, Research Complex at Harwell, Harwell, Oxon OX11 0FA, United Kingdom

Supporting Information

ABSTRACT: Eschewing the common trend toward use of catalysts composed of Cu, it is reported that PdZn alloys are active for CO_2 hydrogenation to oxygenates. It is shown that enhanced CO_2 conversion is achievable through the introduction of Brønsted acid sites, which promote dehydration of methanol to dimethyl ether. We report that deposition of PdZn alloy nanoparticles onto the solid acid ZSM-5, via chemical vapor impregnation affords catalysts for the direct hydrogenation of CO_2 to DME. This catalyst shows dual functionality; catalyzing both CO_2 hydrogenation to methanol and its dehydration to dimethyl in a single catalyst bed, at temperatures of >270 °C. A physically mixed bed comprising 5% Pd 15% Zn/TiO_2 and H-ZSM-5 shows a comparably high performance, affording a dimethyl ether synthesis rate of 546 mmol kg_{cat}^{-1} h^{-1} at a reaction temperature of 270 °C.

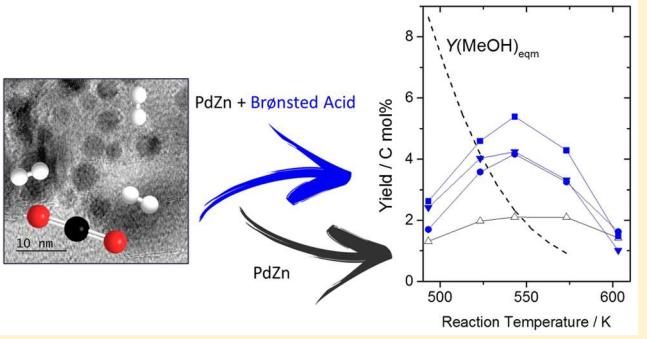

INTRODUCTION

Methanol is ubiquitous within the chemical industry, with global demand exceeding 57 Mt/annum. The majority of this is met through a two-step process whereby synthesis gas is produced via methane steam reforming and then reacted over a $Cu/ZnO/Al_2O_3$ catalyst to prepare methanol. The energy consumption of this process is estimated to exceed 1 exajoule (1×10^{18} J)/annum globally, with a significant carbon footprint (ca. 88 Mt GHG eq).[1] In line with political and social pressure to decrease society's dependence on fossil fuels, there is growing interest in producing methanol through more sustainable routes. One promising route is catalytic CO_2 hydrogenation. The process, however, is restricted by thermodynamic equilibrium; with the reverse water gas shift reaction (RWGS) dominating the reaction at high temperatures. Indeed, methanol is thermodynamically favored at lower temperatures. Unfortunately, because of the relatively low reactivity of CO_2, high reaction temperatures and/or pressures are required for its activation. To maximize yields of value-added products, it is important that CO_2 hydrogenation be carried out near equilibrium. One approach toward circumventing RWGS at elevated reaction temperatures is removal of the product, methanol, from the catalytic system. This can be achieved through dehydration to dimethyl ether (DME), typically over a solid acid catalyst. DME is a key feedstock for production of methylating agents for organic synthesis.[2] DME has also been identified as an environmentally friendly fuel, with low associated emissions of NO_x, hydrocarbons, CO and SO_x.[3] Through the methanol to gasoline (MTG) process, methanol is catalytically converted to yield an equilibrium mixture containing methanol, DME and water. This is then converted to hydrocarbons.[4] Being both exothermic and reversible, methanol dehydration is subject to thermodynamic limitation, though effectively not so under methanol synthesis conditions.[4] Integrating methanol dehydration into CO_2 hydrogenation reaction systems might increase hydrogenation yields, by intercepting the methanol through dehydration to DME, therefore shifting the reaction equilibrium toward methanol formation.

Bifunctional or hybrid catalysts have previously been reported to yield DME through CO_2 hydrogenation, typically consisting of a physical mixture of a traditional Cu-based methanol synthesis catalyst and solid acid catalyst.[5,6] Indeed, most of the studies have focused upon modification of industrial Cu catalysts, with an aim to increase methanol and DME productivities. Physical mixing of methanol synthesis and solid acid catalysts in this way has been reported to afford higher system productivities than where catalysts are spatially segregated as dual fixed beds.[7] Thermodynamic constraints occurred upon separation of methanol synthesis and acid catalysts, with rates limited by methanol synthesis from CO_2.

Received: January 17, 2018
Revised: April 27, 2018
Accepted: May 1, 2018
Published: May 1, 2018

Modification of alumina with niobium has been reported to strongly decrease surface basicity, while slightly increasing its acidity.[8] It is therefore necessary to find a balance between surface basicity and acidity, achieved through optimizing the niobium content. Similarly, it has been reported that physical mixing of Cu-catalysts with γ-Al_2O_3 affords DME as a major product.[9] The solid acid-catalyzed dehydration of methanol to DME has been reported for γ-alumina as well as aluminosilicates and molecular sieves such as ZSM-5,[10] ferrierite[11] and mordenite.[12] Zeolites are unique aluminosilicate materials, offering bidimensional structures, a range of pore sizes and both Brønsted and Lewis surface acidities. Modification of the pore size, acidity and microporous and/or mesoporous structures of zeolite catalysts has been shown to significantly impact upon rates of methanol dehydration.[13] H-ZSM-5 and γ-Al_2O_3 have been used extensively as catalysts for this reaction, with H-ZSM-5 favored due to its relative stability in the presence of water.[14] The hydrophobic/hydrophilic properties of H-ZSM-5 are dependent on the SiO_2/Al_2O_3 ratio and are therefore controllable, with hydrophobic, siliceous isomorphs shown to be less prone to water-mediated deactivation.[15] Additionally, though both Al_2O_3 and H-ZSM-5 possess Lewis acid sites, H-ZSM-5 also contains Brønsted acid sites, which are favorable for methanol dehydration. Juxtaposed with this, however, is the tendency for highly acidic sites within solid acids to promote coke deposition and thereby catalyst deactivation.[16] Two-dimensional zeolite frameworks offer lower resistance to the diffusion of methanol from surface sites on the methanol synthesis catalyst to acid sites on the solid acid catalyst.[17] Additionally, it has been reported that a strong interaction between methanol synthesis and acid catalysts is also important. For example, Cu/ZnO/ZrO supported on a lamellar ferrierite framework showed improved mass transport of methanol into zeolite cavities.[12] Encapsulation of nanoparticles within the pores of a zeolite can also prevent high temperature sintering of nanoparticles during catalytic reactions.[18−20] However, this method can also restrict access of substrates to active sites within micro/mesopores.[20] Therefore, to achieve high DME selectivity, low catalyst acidity would be favorable, limiting formation of coke and byproducts. However, this would, in turn, lower dehydration rates, which are acid site-dependent.[16,21,22]

It has previously been reported that PdZn alloy nanoparticles are active catalysts for the hydrogenation of CO_2 to methanol. Deposition of PdZn onto TiO_2 using solvent-free chemical vapor impregnation (CVI) formed PdZn nanoparticles with a narrow size distribution, which was shown to be beneficial for methanol productivities.[23,24] Activity was shown to be limited by the thermodynamic equilibrium, when reactions were carried out at a temperature of 250 °C. In the current study, dual component, physically mixed catalyst beds are employed. These comprise PdZn/TiO_2 and either H-ZSM-5 or γ-Al_2O_3, with an aim to capture methanol through dehydration to DME. The performance of mixed catalyst beds are then compared with that of PdZn supported directly onto H-ZSM-5 and parametric conditions studied to achieve optimal oxygenate yields.

EXPERIMENTAL SECTION

Catalyst Preparation. All supported catalysts were prepared via chemical vapor impregnation (CVI). A detailed procedure for preparation of 5% PdZn/TiO_2 (1Pd:5Zn mol:mol) (2.0 g) was previously reported. All supported catalysts contain 5 wt % Pd with a Pd:Zn molar ratio of 1:5, which is 15 wt % Zn.[23,24] 5% PdZn (1:5)/ZSM-5 was prepared as follows: $Pd(acac)_2$ (0.29 g, 0.939 mmol) and $Zn(acac)_2$ (1.23 g, 4.698 mmol) were physically mixed with H-ZSM-5 (SiO_2/Al_2O_3 = 30, 1.58 g, Sigma-Aldrich) for 1 min. The dry mixture was transferred to a 50 mL Schlenk flask and then evacuated at room temperature (ca. 10^{-3} bar). Following this, the mixture was heated to 145 °C. After 1 h, the resulting precatalyst was recovered and then calcined in static air (500 °C, 16 h, 10 °C min^{-1}). For characterization studies, a portion of catalyst was subsequently reduced *ex situ* in a flow of 5% H_2/Ar (10 mL min^{-1}, 400 °C, 1 h). For mixed catalyst beds, the required masses of hydrogenation catalyst (5% PdZn(1:5)/TiO_2) and solid acid catalyst (γ-Al_2O_3 (Alfa Aesar) or H-ZSM-5) at 1:1 weight ratios were ground together using pestle and mortar prior to pelleting and sieving ~425−500 μm.

Catalysts were characterized using a range of techniques. Powder X-ray diffraction (XRD) patterns were collected at room temperature using an Enraf Nonus FR590 diffractometer fitted with a hemispherical analyzer, using Cu Kα radiation (l 1/4 1.54 A). X-ray photoelectron spectra (XPS) were recorded on a Kratos Axis Ultra-DLD XPS spectrometer with a monochromatic Al Kα source (75−150 W) and analyzer pass energies of 160 eV (for survey scans) or 40 eV (for detailed scans). Samples were mounted using a double-sided adhesive tape and binding energies referenced to the C (1s) binding energy of adventitious carbon contamination that was taken to be 284.7 eV. Data were analyzed using Casa XPS software. To provide detailed morphological and compositional information at micro and nanoscales, samples were analyzed on a JEOL 2100 (LaB6) high-resolution transmission electron microscopy (HRTEM) system fitted with a high-resolution Gatan digital camera (2k 2k) and a dark held HAADF/Z-contrast detector. Samples were suspended in DI water and ca. 1 μL was added to the TEM grid and dried. Lattice *d*- spacing's were determined using Digital Micrograph software.

NH_3-TPD was carried out using a CHEMBET TPR/TPD chemisorption analyzer, Quantachrome Industries fitted with a TCD. 50 mg of sample was pretreated for 1 h at 130 °C (15 °C min^{-1}) in a flow of helium (80 mL min^{-1}). The sample was then cooled to ambient temperature and ammonia flowed through for 20 min to ensure saturation. The system was then heated 1 h at 100 °C (15 °C min^{-1}) under a flow of helium (80 mL min^{-1}) to remove physisorbed ammonia. Subsequently, chemisorbed ammonia was desorbed by heating to 900 °C (15 °C min^{-1}) in a flow of helium (80 mL min^{-1}) during which period desorbed ammonia was monitored using a TCD, current 180 mV, attenuation 1.

N_2 isotherms were collected on a Micromeritics 3Flex. Samples (ca. 0.050 g) were degassed (150 °C, 6 h) prior to analysis. Analyses were carried out at 77 K with P_0 measured continuously. Free space was measured post- analysis with He. Pore size analysis was carried out using Micromeritics 3Flex software, N_2-Cylindrical Pores- Oxide Surface Model.

CO_2 Hydrogenation Reactions. Catalytic assessments for CO_2 hydrogenation were carried out in a fixed-bed continuous-flow reactor. All quoted gas flows are at STP. The pelleted catalyst (0.5 g, 425−500 μm) was placed without diluent into a stainless tube reactor with internal diameter of 0.5 cm and length 50 cm. Prior to testing, catalysts were prereduced *in situ* in a flow of H_2 gas (30 mL min^{-1}, 1 atm, 400 °C, 1 h) and then cooled to room temperature. The system was then pressurized to 20 bar with reactant gas (1 CO_2:3 H_2:1 N_2 molar ratios),

DOI: 10.1021/acs.iecr.8b00230
Ind. Eng. Chem. Res. 2018, 57, 6821−6829

heated to 250 °C and reaction was carried out for 14 h. A standard reaction gas flow rate of 30 mL min^{-1} was used throughout (GHSV = 3500 h^{-1}). To avoid product condensation, postreactor lines and valves were heated at 130 °C. Products were analyzed via online gas chromatography using an Agilent 7890 system fitted with both FID and TCD detectors. Nitrogen was used as an internal standard.

DME selectivity was calculated based on the following equation:

$$S_{DME} = \frac{(DME_{molmin^{-1}}) \times 2}{\text{Total C in products}_{mol\ min^{-1}}} \times 100$$

RESULTS

Catalyst Characterization. *X-ray Diffraction.* A detailed characterization study was previously reported for 5% PdZn/TiO_2.[23] This catalyst showed stable steady state performance over 24 h online, with high CO_2 conversion (χ = 10.1) and appreciable methanol selectivity (S_{MeOH} = 40%, 1730 mmol kg_{cat}^{-1} h^{-1}) at a temperature of 250 °C and 20 bar reaction pressure.[23] To determine whether this catalyst could function as the CO_2 hydrogenation catalyst in a mixed catalyst bed, binary composites were prepared using the solid acids: γ-Al_2O_3 and H-ZSM-5 (30). For comparison, 5% PdZn/ZSM-5 (30) was prepared via chemical vapor impregnation, CVI method. Following impregnation with Pd and Zn acetylacetonate precursors by CVI, all catalysts were calcined in air (16 h, 500 °C). Following this, the XRD diffractogram for 5% PdZn/ZSM-5 (Figure 1a) is comparable to that of the H-ZSM-5 support (JCPDS 44-0003), with the addition of a peak at 34°. This consistent with formation of a ZnO phase (JCPDS 36-1451).[25] Following reduction of this catalyst (400 °C, 3 h, 5% H_2/Ar) the ZnO diffraction peak at 34° becomes narrower and decreases in intensity (Figure 1d). Formation of a PdZn alloy is indicated by peaks at 40° and 44°, corresponding to PdZn(111) and PdZn(200) crystal planes.[26,27] This indicates the reduction of ZnO at an interface with Pd to form the PdZn alloy, possibly promoted via hydrogen spillover from Pd sites.

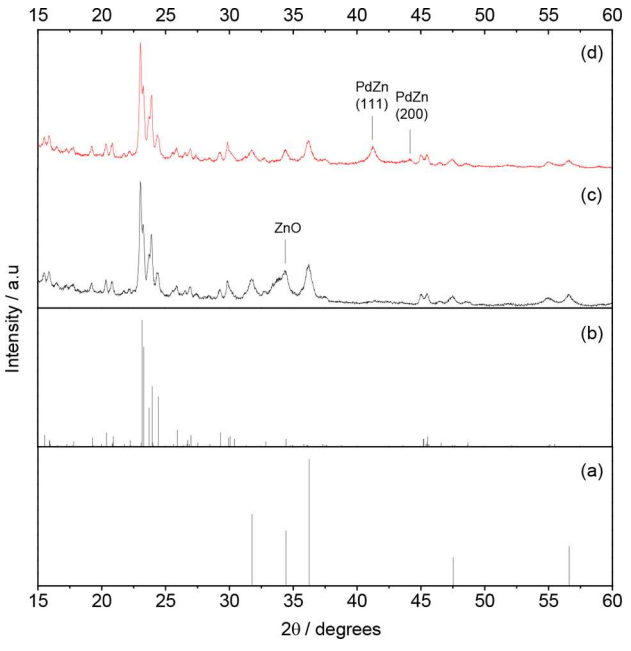

Figure 1. Normalized diffraction lines for (a) ZnO (CCDC 00-036-1451) and (b) H-ZSM-5 (30)(CCDC 00-042-0023) and XRD diffractograms for 5% PdZn/ZSM-5 (30) following either (c) calcination in air at 500 °C or (d) reduction in 5% H/Ar at 400 °C.

N_2 Physisorption. N_2 physisorption analyses were carried out on unmodified H-ZSM-5 (following calcination in air at 500 °C, 16 h) and 5% PdZn/ZSM-5 both prior to and following catalyst assessment. N_2 adsorption isotherms and BET plots are shown in Figure 2.

A decrease in BET surface area was observed following deposition of Pd and Zn onto H-ZSM-5 (30) via CVI, from 401 m^2 g^{-1} for the zeolite support to 334 m^2 g^{-1}. This equated to a 16.5% decrease in surface area, which might be attributed to the total metal loading of Pd/Zn, which equaled 20 wt %. A corresponding decrease in micropore volume was also observed, from 0.163 to 0.131 cm^3 g^{-1} (Table 1, Entries 1 and 2). Following catalytic testing at 270 °C, 20 bar for 11 h, a decrease in BET surface area to 300 m^2 g^{-1} was observed, with a corresponding decrease in micropore volume to 0.123 cm^3 g^{-1}. Given the sample preparation conditions, it is unlikely that this decrease in surface area/pore volume is due to product retention within the zeolite pores. Alternately, this this physical change might be attributed to coking of the acidic zeolite catalyst during dehydration of methanol to DME, which is well documented;[28,29] however, TGA analysis in air of fresh and used catalysts showed no significant mass loss attributable to combustion of carbonaceous residues (Figure S1).

X-ray Photoelectron Spectroscopy. XPS allowed for surface-specific analysis of the supported catalysts, to confirm formation of PdZn alloy nanoparticles on ZSM-5. Following annealing in air, the XPS spectrum (Figure 3ai) shows a clear Pd 3d peak at 337 eV, indicating the presence of PdO on the surface.[30] Subsequent annealing in hydrogen at 400 °C led to a pronounced peak shift toward lower binding energies (Figure 3aii), indicating changes in the PdO electronic properties and formation of a PdZn alloy.[31,32] This was further supported by Zn LMM Auger electron spectra, which show a peak at 995 eV in Figure 3bii following reductive heat treatment. Though this peak was previously identified as metallic Zn species on the surface,[33,34] in the case of this catalyst a more plausible explanation is formation of a PdZn alloy.[23]

Transmission Electron Microscopy. TEM was used to determine the particle size distribution of PdZn nanoparticles in 5% PdZn/TiO_2, 5% PdZn/ZSM-5 (30) and physically mixed 5% PdZn/TiO_2/ZSM-5 catalysts. Micrographs representative of the catalysts prior to and following catalyst assessment for CO_2 hydrogenation are shown in Figure 4. Following heat treatment at 400 °C in H_2/Ar, 5% PdZn/TiO_2 shows an average PdZn diameter of 3.9 nm (Figure 4a). This catalyst was then pelleted with H-ZSM-5 (30) to form a composite catalyst, prior to testing in CO_2 hydrogenation. The used catalyst was recovered and analyzed by TEM. No change in average PdZn particle size was observed, with the mean particle size maintained at 3.9 nm (Figure 4b).

TEM micrographs representative of 5% PdZn/ZSM-5 (30) following annealing in hydrogen at 400 °C show a homogeneous distribution and average PdZn diameter of 5.5 nm (Figure 4c). This was observed to increase to 6.1 nm following catalytic assessment (270 °C, 20 bar, 14 h) (Figure 4d). Identification of supported nanoparticles as being PdZn alloy was confirmed through HRTEM analysis of 5% PdZn/TiO_2 with measurement of lattice spacings (Figure S2).

DOI: 10.1021/acs.iecr.8b00230
Ind. Eng. Chem. Res. 2018, 57, 6821−6829

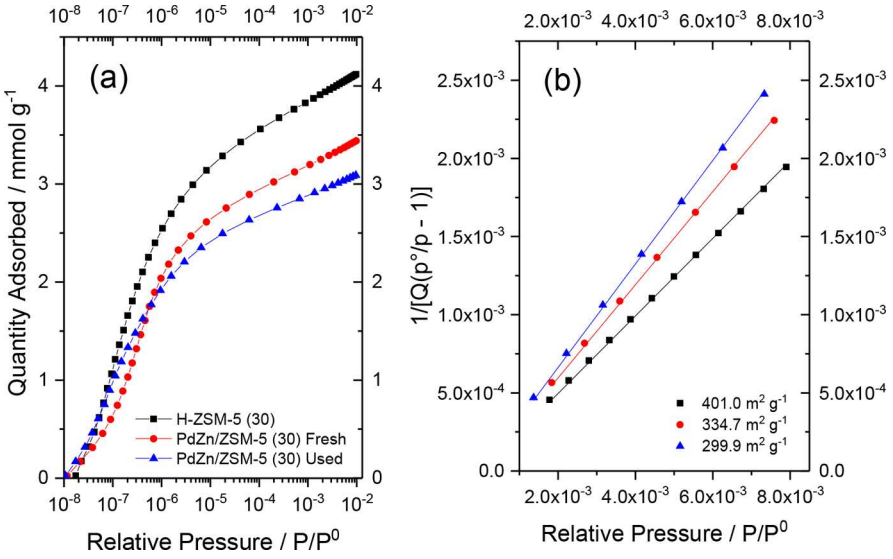

Figure 2. N_2 physisorption isotherms (a) and BET plots (b) for H-ZSM-5 (30), freshly prepared 5% PdZn/ZSM-5 (30) and 5% PdZn/ZSM-5 (30) following catalyst assessment.

Table 1. Physicochemical Properties of Zeolite Catalysts

Entry	Reduction conditions[a]	PdZn size (nm)[b]	BET surface area (m^2 g^{-1})[c]	Micropore volume (cm^3g^{-1})
1	H-ZSM-5		401.0	0.163
2	5% PdZn/ ZSM-5	5.5	334.7	0.131
3	5% PdZn/ ZSM-5, post	6.1	299.9	0.123

[a]All catalysts were precalcined (500 °C, 10 °C min^{-1}, 16 h). [b]Determined by TEM. [c]Determined by N_2 physisorption.

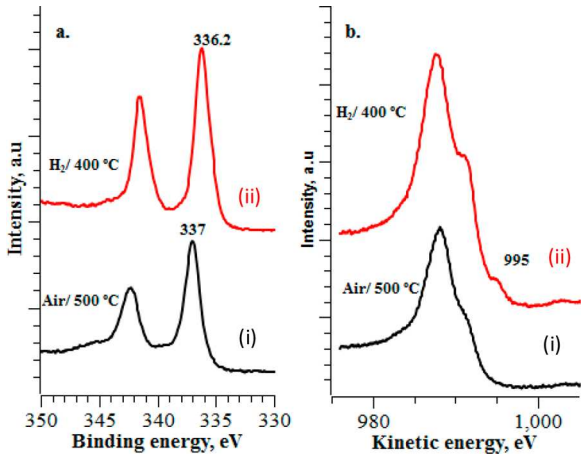

Figure 3. Pd 3d XP spectra (a) and Zn LMM Auger electron spectra (b) of 5% PdZn/ZSM-5 following air calcination at 500 °C and H_2 reduction at 400 °C.

Surface Acidity. Brønsted acidity is key in increasing oxygenated product yields through catalytic dehydration of methanol to DME. N_2 adsorption studies on PdZn/ZSM-5 catalyst indicated that coke forms upon the catalyst *in situ*. It should also be noted that the reaction yields 3 equiv H_2O per 1 equiv DME formed from CO_2 and that dealumination of zeolites such as ZSM-5 can occur upon thermal treatment in the presence of H_2O. To determine whether the acid properties of the ZSM-5 support undergo change during CO_2 hydrogenation, NH_3-TPD analysis was carried out on PdZn/ZSM-5 both prior to and following catalytic testing. For comparison, H-ZSM-5 was also analyzed.

H-ZSM-5 (30) (Figure 5a) presents two distinct NH_3 desorptions, centered at 280 and 440 °C. The lower temperature desorption is attributed to adsorption at weak acid sites (Brønsted and Lewis) with the high temperature desorption unequivocally assigned to NH_3 chemisorbed at strongly acidic Brønsted sites.[35−37] Deposition of Pd(5 wt %) and Zn (15 wt %) onto the zeolite support effected a significant change in the NH_3-TPD profile (Figure 5b). Indeed, a clear decrease in peak intensity is observed for the desorption centered at 440 °C. This suggests either exchange of cationic Pd/Zn species or blocking of acid sites by supported nanoparticles. Overlapping desorptions at temperatures of >500 °C might be assigned to desorption of ammonia decomposition products from surface oxides, for example ZnO, which was observed in the XRD of this catalyst (Figure 1a). Indeed, such high temperature desorptions from ZnO have previously been attributed to desorption of NH_n species, formed through dissociative adsorption of ammonia.[38] An increase in the low temperature desorption event following catalytic testing (Figure 5c) could indicate formation of Lewis acid sites either during the catalyst pretreatment or CO_2 hydrogenation reaction. Meanwhile, the high temperature desorption profile in Figure 5c is comparable with that of the unused catalyst. Given that the XRD pattern exhibited a less intense peak for ZnO (Figure 1b) following testing, these data suggest that discrete ZnO nanoparticles might remain within the zeolite pores following catalytic testing. Previous studies have reported that dehydration of methanol to yield DME occurs at moderate-strength acid sites.[22]

Catalytic Performance. The catalytic activity of PdZn catalysts in the simultaneous (i) hydrogenation of CO_2 to methanol and (ii) dehydration of methanol to DME was assessed at 270 °C. Two approaches were taken, specifically (i) mixing of a 5% PdZn(1:5)/TiO_2 catalyst with solid acids (γ-Al_2O_3/ZSM-5) at 1:1 weight ratios and (ii) deposition of PdZn onto a Brønsted acidic solid acid support (ZSM-5). Table 2 shows steady state catalytic data obtained at 20 bar and a reaction temperature of 270 °C. Optimal methanol yields have previously been reported at 250 °C for 5% PdZn/TiO_2, with

DOI: 10.1021/acs.iecr.8b00230
Ind. Eng. Chem. Res. 2018, 57, 6821−6829

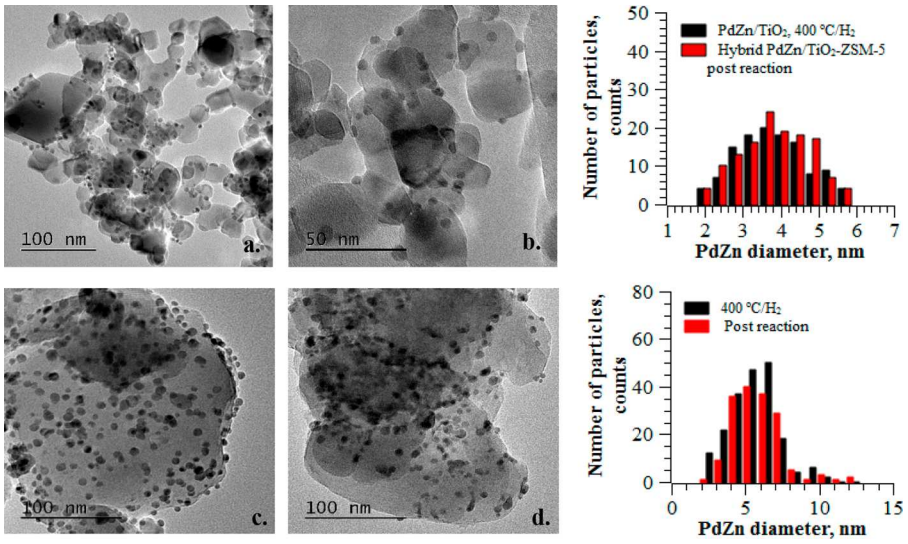

Figure 4. TEM micrographs and corresponding particle size distributions for (a) 5% PdZn/TiO_2 reduced in H_2 at 400 °C, (b) postreaction mixed 5% PdZn/TiO_2/ZSM-5 catalysts, (c) 5% PdZn/ZSM-5 after annealing at 400 °C in H_2 and (d) 5% PdZn/ZSM-5 following CO_2 hydrogenation.

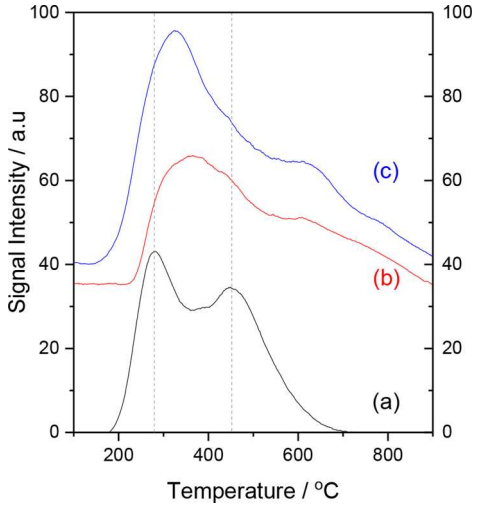

Figure 5. NH_3-TPD profiles for (a) H-ZSM-5 (30), (b) 5% PdZn/ZSM-5 before catalytic testing and (c) 5% PdZn/ZSM-5 following catalytic testing.

high CO selectivities observed at temperatures of >250 °C due to domination by RWGS. The same catalyst showed 13% CO_2 conversion and methanol/CO selectivities of 13% and 87% respectively at 270 °C (Table 2, Entry 1). A significant shift in the product distribution was observed when 5% PdZn (1:5)/TiO_2 was copelleted with solid acids, either Al_2O_3 or ZSM-5 (30) (Table 2, Entries 2 and 3). For the latter, a decrease in CO_2 conversion to 11% was observed. Addition of ZSM-5 effected a significant increase in DME selectivity, which increased from 0.2% for 5% PdZn (1:5)/TiO_2 to 32%. This equated to a DME synthesis rate of ca. 667 $mmol_{DME}$ kg_{cat}^{-1} h^{-1}. This shift in reaction selectivity clearly shows the ability of H-ZSM-5 (30) to catalyze the dehydration of methanol to DME. Addition of Al_2O_3 also afforded an increase in DME selectivity, to 29% (527 mmol kg_{cat}^{-1} h^{-1}), with CO_2 conversion (14%) (Table 2, Entry 2). Impregnation of H-ZSM-5 (30) with PdZn via CVI provided information as to the importance of spatial separation of the active sites for CO_2 hydrogenation and methanol dehydration reactions. This catalyst was active for CO_2 hydrogenation (Table 2, Entry 4), with far higher DME selectivity (30%) than was observed for the analogous 5% PdZn (1:5)/TiO_2 catalyst in Table 2. This equated to a DME synthesis rate of 544 mmol kg_{cat}^{-1} h^{-1}. This shows the advantage of using a mixed, composite catalyst. 5% PdZn/TiO_2-Al_2O_3 also showed dimethyl ether formation, at 527 mmol kg_{cat}^{-1} h^{-1}. This shows that the efficiency of methanol dehydration to dimethyl ether over Al_2O_3 is comparable to ZSM-5 despite the surface area of H-ZSM-5 (30) (400 m^2 g^{-1}) being far higher than Al_2O_3 (70 m^2 g^{-1}).

Effect of Reaction Temperatures on CO_2 Conversion and DME Synthesis Rates. The rate of CO_2 hydrogenation is strongly dependent upon reaction temperature and pressure. Since the aim of this work is to achieve CO_2 hydrogenation under mild reaction conditions, the pressure was maintained at 20 bar as opposed to the 50 bar currently used in industrial methanol synthesis processes. Figure 6a shows the effect of

Table 2. Steady State Catalytic Performance of PdZn Catalysts for CO_2 Hydrogenation Reaction at 270 °C

Entry[a]	Catalyst	χ CO_2 (%)	S(CH_3OCH_3) (%)	S(CH_3OH) (%)	S(CO) (%)	S(CH_4) (%)	mmol CH_3OCH_3 (kg_{cat}^{-1} h^{-1})	mmol CH_3OH (kg_{cat}^{-1} h^{-1})	C balance (%)
1	PdZn/TiO_2	13	0.2	13.2	86.6	0.02	4	609	102
2	PdZn/TiO_2 + Al_2O_3	14	29.1	4.3	66.6	0.02	527	155	101
3	PdZn/TiO_2 + ZSM-5	11	32.3	5.9	61.7	0.05	667	245	102
4	PdZn/ZSM-5	14	30.4	4.2	65.3	0.02	544	147	101
5	Cu/ZnO/Al_2O_3	18	0	16.6	83.4	0	0	754	99

[a]Entries 1–4 were prereduced *in situ* (400 °C, H_2, 1 h, 30 mL min^{-1}, 1 bar) prior to reaction. Data was obtained at steady state after 10 h of reaction. Entry 5, Cu/ZnO/Al_2O_3 (Alfa Aesar product no. 45776), prereduced *in situ* (1 h at 220 °C, 2 °C min^{-1}, 30 mL min^{-1} of 5% H_2/He, 1 bar).

DOI: 10.1021/acs.iecr.8b00230
Ind. Eng. Chem. Res. 2018, 57, 6821–6829

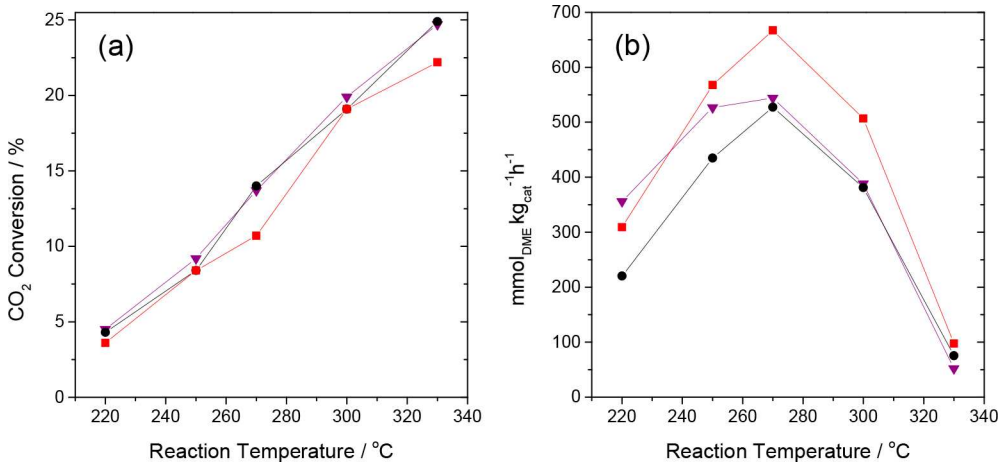

Figure 6. CO_2 conversion (a) and DME productivities (b) for (purple ▼) 5% PdZn/ZSM-5 and physically mixed composite catalyst beds containing 5% PdZn/TiO_2 and either (●) γ-Al_2O_3 or (red ■) H-ZSM-5.

Table 3. Catalytic Performance of 5% PdZn/ZSM-5 (30) at Reaction Temperatures of 220−330 °C

Temp (°C)	χ CO_2 (%)	S(CH_3OCH_3) (%)	S(CH_3OH) (%)	S(CO) (%)	S(CH_4) (%)	mmol CH_3OCH_3 (kg_{cat}^{-1} h^{-1})	mmol CH_3OH (kg_{cat}^{-1} h^{-1})	mmol CO (kg_{cat}^{-1} h^{-1})	mmol CH_4 (kg_{cat}^{-1} h^{-1})	C balance (%)
220	4.5	59.8	5.4	34.8	0.02	356	64	415	0.2	102
250	9.2	41.2	4.5	54.3	0.02	527	114	1390	0.6	102
270	13.7	30.4	4.2	65.3	0.01	544	147	2323	1.1	101
300	19.9	15.2	3.7	81.1	0.04	388	190	4130	2.5	100
330[a]	24.7	1.7	3.0	95.2	0.05	52	190	5945	4.1	99

[a]At 330 °C, C_2 products were detected but not quantified. These are excluded from selectivity calculations.

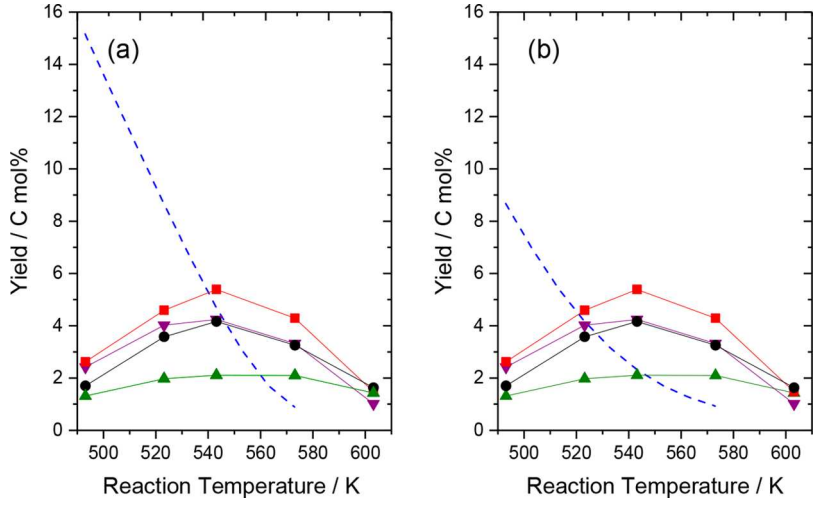

Figure 7. Comparison of steady state oxygenate yields (combined DME and MeOH yields/C-mol %) with theoretical equilibrium yields of (a) DME and (b) MeOH from CO_2 hydrogenation (also as C-mol %). (green ▲) PdZn/TiO_2, (●) PdZn/TiO_2-Al_2O_3, (red ■) PdZn/TiO_2-H-ZSM-5 and (purple ▼) PdZn/ZSM-5, (--) equilibrium yield in C-mol %.

varying the reaction temperature from 220 to 330 °C at a constant 20 bar reactor pressure. All catalyst beds showed nominal activity at 220 °C, affording ca. 3−4% CO_2 conversion. CO_2 conversion increases significantly at temperatures of >250 °C.

Figure 6b shows dimethyl ether production rates across the same range of reaction temperatures. 5% PdZn/ZSM-5 showed a steady state DME productivity of 356 $mmol_{DME}$ kg_{cat}^{-1} h^{-1} at 220 °C, which was higher than the rates observed over mixed catalyst beds. Increasing the reaction temperature to 250 °C had a beneficial effect upon rates of DME formation, which may result from high methanol productivity on PdZn sites coupled with efficient methanol dehydration.

Between 250 and 270 °C, physically mixed 5% PdZn/TiO_2-ZSM-5 showed higher DME synthesis rates than 5% PdZn/ZSM-5. Further increasing the temperature, to 330 °C, led to significant decreases in DME productivity, despite increasing CO_2 conversion. This is the result of increased CO selectivities and ZSM-5-catalyzed conversion of methanol to C_2 compounds at 330 °C. Table 3 shows steady state metrics for 5% PdZn/ZSM-5 (30) at reaction temperatures of 220−330 °C. Methanol and DME selectivity decrease with increasing

DOI: 10.1021/acs.iecr.8b00230
Ind. Eng. Chem. Res. 2018, 57, 6821−6829

temperature. A corresponding increase in selectivity toward CO and methane was observed across the same range. Formation of C_2 hydrocarbons was observed at a reaction temperature of 330 °C; however, due to analytical constraints, these were not quantified in the current study. Hydrocarbons were therefore not considered when quantifying product selectivities and the carbon balance at 330 °C. These observations do however indicate that Brønsted acidic PdZn catalysts are active for single-step conversion of CO_2 to hydrocarbons at 330 °C.

The aim of coupling PdZn CO_2 hydrogenation and solid acid catalysts is to increase total oxygenate yields, especially at reaction temperatures of >250 °C. Total oxygenate yields were calculated as a sum of DME yield (C-mol %) and MeOH yield (C-mol %) for PdZn catalysts. These were compared to (a) DME and (b) MeOH yields calculated at thermodynamic equilibrium in a previous study by Shen et al., which considered both CO_2 hydrogenation (to either MeOH or DME) and RWGS reactions[39] (note, literature equilibrium yields adjusted to $P(H_2{:}CO_2$ 3:1) = 16 bar to allow comparison with reaction data whereby a $P(N_2)$ = 4 bar is employed as internal standard). As shown in Figure 7, with increasing temperature (to 330 °C) Total oxygenate yields (presented as C-mol %) over 5% PdZn/TiO_2 first increased and then decreased. The RWGS reaction comes to dominate the reaction, yielding CO. This might indicate that methanol undergoes high temperature oxidation to CO/H_2 on the TiO_2 surface. Previous TPD studies have reported that CH_3OH undergoes decomposition to CO and H_2O over TiO_2 at temperatures of ca. 300 °C.[40] As shown in Figure 7, the performance of all the catalysts was kinetically limited at low temperatures. Of the catalyst beds tested, 5% PdZn/TiO_2-H-ZSM-5 shows the highest overall oxygenate yield at the lowest reaction temperature of 220 °C. This suggests that the surface hydroxyl vacancies on TiO_2 facilitate low temperature CO_2 hydrogenation and the H-ZSM-5 further catalyzes methanol dehydration to DME. Addition of Brønsted acidity significantly improved oxygenate yields. Indeed, through addition of either Al_2O_3 or ZSM-5 to PdZn/TiO_2 or deposition of PdZn directly onto ZSM-5, total oxygenate yields exceeded the theoretical equilibrium yields of MeOH at reaction temperatures of >250 °C (Figure 7b) and theoretical DME equilibrium yields at temperatures of >270 °C (Figure 7a). It should however be noted that the study by Shen et al. considered CO yields and either DME (Figure 7a) or MeOH (Figure 7b) yields, whereas reaction data (C-mol % yields) plots in Figure 7a,b represent summed MeOH and DME yields.

Assessing the Stability of 5% PdZn/ZSM-5. The catalytic stability of 5% PdZn/ZSM-5 was assessed at steady state for 11 h at 270 °C, 20 bar. As shown in Figure 8, steady state conversion of CO_2 is maintained over 11 h of reaction. Product selectivities remain at steady state, affording ca. 30% DME selectivity and 65% CO selectivity at ca. 14% CO_2 conversion. Steady state methanol selectivity was 4.2% and the ratio of DME:CH_3OH was maintained throughout the 11 h testing period, indicating that the water vapor formed in CO_2 hydrogenation and methanol dehydration reactions is not affecting an online deactivation of the catalyst.

■ DISCUSSION

The hydrogenation of CO_2 to methanol was previously reported for 5% PdZn/TiO_2 catalysts, with PdZn identified as the active site for methanol formation.[23,24] It is clear from Figure 7 that through supporting of PdZn nanoparticles onto ZSM-5, it is possible to promote a higher yielding conversion of

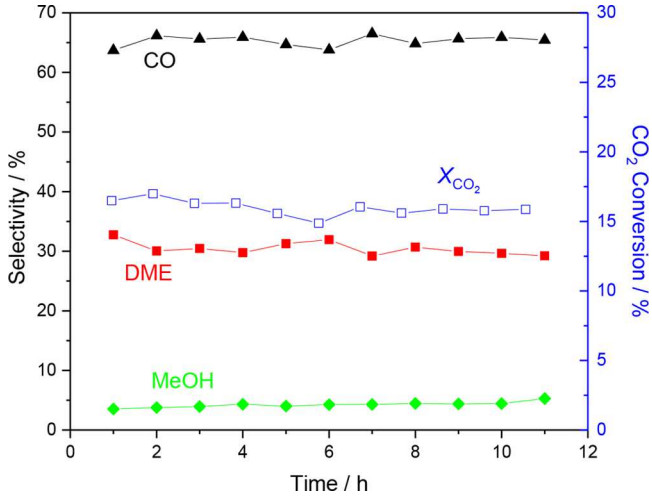

Figure 8. Catalytic performance of 5% PdZn/ZSM-5 in hydrogenation of CO_2 to DME over 11 h. (blue □) CO_2 conversion, ▲ CO selectivity, (red ■) selectivity DME, (green ◆) MeOH selectivity.

CO_2 to oxygenated products; methanol and DME. Conversion of CO_2 to DME has the added benefit of lowering the rate of the RWGS reaction at higher temperatures, with lower CO productivities observed than for 5% PdZn/TiO_2 catalysts. Increased methane productivities were observed over 5% PdZn/ZSM-5 however, when compared with 5% PdZn/TiO_2. Methane is derived through direct methanation of either CO_2 or methanol. Though supported PdZn alloy species enhance methanol formation, regardless of the support used, deposition onto ZSM-5 yields bifunctionality, catalyzing formation of both methanol and subsequently DME. DME can be produced through either (i) direct hydrogenation of CO_2 to DME (eq 1) or (ii) hydrogenation of CO_2 to methanol with subsequent methanol dehydration (eqs 2−4). The general mechanism for methanol dehydration involves reaction between two methanol molecules and an acid catalyst (eq 4). Methanol dehydration follows two different routes, either (i) associative or (ii) methoxy-mediated dissociative that occurs on Brønsted acid sites, depending on the temperature and pressure of the catalytic system[41] that the preferred routes depend on the methanol pressure.[42] At high partial pressures of methanol, adsorbed methanol is stabilized through dimer formation. This dimer can itself undergo subsequent dehydration to form DME. With increasing methanol partial pressure, dissociation of the H-bonded methanol is reported to be less favorable due to this dimer formation.[42]

The dehydration of methanol to DME may also yield methane and coke as byproducts,[43,44] which could cause catalyst deactivation at long times on stream (≫11 h). Methanation occurs when methoxy species strongly bond to acidic surface sites, creating surface formates, which decompose to form CO, H_2 and CH_4.[45] Relatively high CO_2 conversion and oxygenate productivities were observed for catalyst beds comprising of PdZn and solid acid catalysts. Indeed, all acidic catalyst beds show high productivities toward methanol and DME synthesis relative to PdZn/TiO_2, with total oxygenate productivities coming to exceed the calculated equilibrium DME or MeOH yields at elevated temperatures.[39] However, DME selectivity decreased significantly at temperatures of >300 °C. This suggests that methanol undergoes additional reactions at elevated temperatures, for example catalytic cracking or coking.[46] In general, the composite PdZn/TiO_2-ZSM-5 bed

DOI: 10.1021/acs.iecr.8b00230
Ind. Eng. Chem. Res. 2018, 57, 6821−6829

afforded higher oxygenates yields across the temperature range studied than did PdZn/ZSM-5 (Figure 7). This might be attributed to occupation or blocking of Brønsted acid sites when PdZn is deposition onto ZSM-5 via CVI. PdZn might also restrict access of methanol to the ZSM-5 micropores. As shown in Table 1, a decrease in mass-normalized BET surface area and pore volume is observed following deposition of PdZn on H-ZSM-5. This is consistent with the total metal loading (20 wt %, 5% Pd, 15% Zn). A corresponding decrease in acid site density was observed in NH_3-TPD studies in Figure 5. On the other hand, the composite, physically mixed PdZn/TiO_2-ZSM-5 catalyst avoids this effect, with the zeolite's acid site density unaffected. This indicates that while the methanol synthesis and solid acid catalysts must be in a close proximity, to allow for diffusion of the methanol to acid sites, there is no apparent restriction of methanol diffusing from the surface of PdZn/TiO_2 to acid sites in nearby H-ZSM-5 crystallites. The average PdZn diameter observed for 5% PdZn/ZSM-5 (5.5 nm) is significantly larger than that of the analogous TiO_2 catalyst (3.9 nm). Given that previous studies on PdZn/TiO_2 and Pd/ZnO have highlighted a positive relationship between decreasing PdZn particle size and increasing CO_2 hydrogenation rates,[23,24,47] a decrease in the average particle size of ZSM-5-supported PdZn species might be expected to yield increased catalyst productivities.

$$2CO_2 + 6H_2 \rightarrow CH_3OCH_3 + 3H_2O \quad \Delta H_{298} = -122.2\ \text{kJ mol}^{-1} \tag{1}$$

$$CO_2 + 3H_2 \rightarrow CH_3OH + H_2O \quad \Delta H_{298} = -49.46\ \text{kJ mol}^{-1} \tag{2}$$

$$CO_2 + H_2 \rightarrow CO + H_2O \quad \Delta H_{298} = 41.17\ \text{kJ mol}^{-1} \tag{3}$$

$$2CH_3OH \rightarrow CH_3OCH_3 + H_2O \quad \Delta H_{298} - 23.43\ \text{kJ mol}^{-1} \tag{4}$$

CONCLUSIONS

In the current study, the catalytic activities of supported PdZn alloy catalysts have been assessed. Through deposition of PdZn onto a solid Brønsted acid; ZSM-5, or mixing and copelleting of PdZn/TiO_2 and either H-ZSM-5 or Al_2O_3 enhanced CO_2 conversions might be achieved. Indeed, a mixed bed comprising 5% PdZn/TiO_2-ZSM-5 exhibited high CO_2 conversion of 11% and selectivity toward DME of 32% at a reaction temperature of 270 °C and 20 bar pressure. At reaction temperatures of >270 °C, observed total oxygenate yields exceeded those expected, based upon previously reported thermodynamic equilibrium yields of DME or MeOH. The catalytic performance of mixed PdZn/TiO_2-ZSM-5 is broadly superior to that of PdZn/ZSM-5 catalysts and this difference is ascribed to blocking of crucial Brønsted acid sites when PdZn is directly supported upon the zeolite surface, which also leads to decreased mass-normalized BET surface area as deposited metals account for 20 wt % of the PdZn/ZSM-5 catalyst.

ASSOCIATED CONTENT

Supporting Information

The Supporting Information is available free of charge on the ACS Publications website at DOI: 10.1021/acs.iecr.8b00230.

Thermogravimetric analyses and HRTEM micrographs (PDF)

AUTHOR INFORMATION

Corresponding Authors

*H. Bahruji. E-mail: BahrujiH@Cardiff.ac.uk.

*R. D. Armstrong. E-mail: ArmstrongR4@Cardiff.ac.uk.

ORCID

Robert D. Armstrong: 0000-0001-9075-3492

Michael Bowker: 0000-0001-5075-1089

Graham J. Hutchings: 0000-0001-8885-1560

Notes

The authors declare no competing financial interest.

ACKNOWLEDGMENTS

Authors would like to acknowledge UK Catalysis Hub for H. Bahruji. UK Catalysis Hub is kindly thanked for resources and support provided via our membership of the UK Catalysis Hub Consortium and funded by EPSRC (grants EP/K014706/1, EP/K014668/1, EP/K014854/1, EP/K014714/1 and EP/M013219/1). EPSRC grant EP/N010531/1 is also acknowledged. This contribution was identified by Zili Wu (Oak Ridge National Laboratory, USA), Matteo Cargnello (Stanford University, USA), and Sen Zhang (University of Virginia, USA) as the Best Presentation (R. D. Armstrong) in the "Cooperative Catalysis at Surfaces & Interfaces: Impact on Chemistry & Energy Frontiers" session of the 2017 ACS Fall National Meeting in Washington, D.C.

REFERENCES

(1) DECHEMA Technology Roadmap "Energy and GHG Reductions in the Chemical Industry via Catalytic Processes". http://dechema.de/en/industrialcatalysis.html (accessed 12/01/2018).

(2) Hutchings, G. J.; Hunter, R. Hydrocarbon formation from methanol and dimethyl ether: a review of the experimental observations concerning the mechanism of formation of the primary products. *Catal. Today* **1990**, *6* (3), 279−306.

(3) Semelsberger, T. A.; Borup, R. L.; Greene, H. L. Dimethyl ether (DME) as an alternative fuel. *J. Power Sources* **2006**, *156* (2), 497−511.

(4) Diep, B. T.; Wainwright, M. S. Thermodynamic equilibrium constants for the methanol-dimethyl ether-water system. *J. Chem. Eng. Data* **1987**, *32* (3), 330−333.

(5) An, X.; Zuo, Y.-Z.; Zhang, Q.; Wang, D.-z.; Wang, J.-F. Dimethyl Ether Synthesis from CO2 Hydrogenation on a CuO−ZnO−Al2O3−ZrO2/HZSM-5 Bifunctional Catalyst. *Ind. Eng. Chem. Res.* **2008**, *47* (17), 6547−6554.

(6) Zhao, Y.; Chen, J.; Zhang, J. Effects of ZrO2 on the Performance of CuO-ZnO-Al2O3/HZSM-5 Catalyst for Dimethyl Ether Synthesis from CO2 Hydrogenation. *J. Nat. Gas Chem.* **2007**, *16* (4), 389−392.

(7) Bonura, G.; Cordaro, M.; Spadaro, L.; Cannilla, C.; Arena, F.; Frusteri, F. Hybrid Cu−ZnO−ZrO2/H-ZSM5 system for the direct synthesis of DME by CO2 hydrogenation. *Appl. Catal., B* **2013**, *140−141*, 16−24.

(8) Lima, S. H.; Forrester, A. M. S.; Amparo Palacio, L.; Faro, A. C., Jr Niobia-alumina as methanol dehydration component in mixed catalyst systems for dimethyl ether production from syngas. *Appl. Catal., A* **2014**, *488*, 19−27.

(9) Suwannapichat, Y.; Numpilai, T.; Chanlek, N.; Faungnawakij, K.; Chareonpanich, M.; Limtrakul, J.; Witoon, T. Direct synthesis of dimethyl ether from CO2 hydrogenation over novel hybrid catalysts containing a CuZnOZrO2 catalyst admixed with WOx/Al2O3 catalysts: Effects of pore size of Al2O3 support and W loading content. *Energy Convers. Manage.* **2018**, *159*, 20−29.

DOI: 10.1021/acs.iecr.8b00230
Ind. Eng. Chem. Res. 2018, 57, 6821−6829

(10) Liu, R.-w.; Qin, Z.-z.; Ji, H.-b.; Su, T.-m. Synthesis of Dimethyl Ether from CO2 and H2 Using a Cu−Fe−Zr/HZSM-5 Catalyst System. *Ind. Eng. Chem. Res.* **2013**, *52* (47), 16648−16655.
(11) Bonura, G.; Cannilla, C.; Frusteri, L.; Mezzapica, A.; Frusteri, F. DME production by CO2 hydrogenation: Key factors affecting the behaviour of CuZnZr/ferrierite catalysts. *Catal. Today* **2017**, *281* (Part 2), 337−344.
(12) Bonura, G.; Frusteri, F.; Cannilla, C.; Drago Ferrante, G.; Aloise, A.; Catizzone, E.; Migliori, M.; Giordano, G. Catalytic features of CuZnZr−zeolite hybrid systems for the direct CO2-to-DME hydrogenation reaction. *Catal. Today* **2016**, *277* (Part 1), 48−54.
(13) Catizzone, E.; Aloise, A.; Migliori, M.; Giordano, G. Dimethyl ether synthesis via methanol dehydration: Effect of zeolite structure. *Appl. Catal., A* **2015**, *502*, 215−220.
(14) Laugel, G.; Nitsch, X.; Ocampo, F.; Louis, B. Methanol dehydration into dimethylether over ZSM-5 type zeolites: Raise in the operational temperature range. *Appl. Catal., A* **2011**, *402* (1), 139−145.
(15) Nakamoto, H.; Takahashi, H. Hydrophobic natures of zeolite ZSM-5. *Zeolites* **1982**, *2* (2), 67−68.
(16) Fu, Y.; Hong, T.; Chen, J.; Auroux, A.; Shen, J. Surface acidity and the dehydration of methanol to dimethyl ether. *Thermochim. Acta* **2005**, *434* (1), 22−26.
(17) Opanasenko, M. V.; Roth, W. J.; Cejka, J. Two-dimensional zeolites in catalysis: current status and perspectives. *Catal. Sci. Technol.* **2016**, *6* (8), 2467−2484.
(18) Gu, J.; Zhang, Z.; Hu, P.; Ding, L.; Xue, N.; Peng, L.; Guo, X.; Lin, M.; Ding, W. Platinum Nanoparticles Encapsulated in MFI Zeolite Crystals by a Two-Step Dry Gel Conversion Method as a Highly Selective Hydrogenation Catalyst. *ACS Catal.* **2015**, *5* (11), 6893−6901.
(19) Laursen, A. B.; Højholt, K. T.; Lundegaard, L. F.; Simonsen, S. B.; Helveg, S.; Schüth, F.; Paul, M.; Grunwaldt, J.-D.; Kegnæs, S.; Christensen, C. H.; Egeblad, K. Substrate Size-Selective Catalysis with Zeolite-Encapsulated Gold Nanoparticles. *Angew. Chem., Int. Ed.* **2010**, *49* (20), 3504−3507.
(20) Farrusseng, D.; Tuel, A. Perspectives on zeolite-encapsulated metal nanoparticles and their applications in catalysis. *New J. Chem.* **2016**, *40* (5), 3933−3949.
(21) Catizzone, E.; Aloise, A.; Migliori, M.; Giordano, G. Dimethyl ether synthesis via methanol dehydration: Effect of zeolite structure. *Appl. Catal., A* **2015**, *502* (Supplement C), 215−220.
(22) Li, H.; He, S.; Ma, K.; Wu, Q.; Jiao, Q.; Sun, K. Micro-mesoporous composite molecular sieves H-ZSM-5/MCM-41 for methanol dehydration to dimethyl ether: Effect of SiO2/Al2O3 ratio in H-ZSM-5. *Appl. Catal., A* **2013**, *450* (Supplement C), 152−159.
(23) Bahruji, H.; Bowker, M.; Jones, W.; Hayward, J.; Ruiz Esquius, J.; Morgan, D. J.; Hutchings, G. J. PdZn catalysts for CO2 hydrogenation to methanol using chemical vapour impregnation (CVI). *Faraday Discuss.* **2017**, *197* (0), 309−324.
(24) Bahruji, H.; Esquius, J. R.; Bowker, M.; Hutchings, G.; Armstrong, R. D.; Jones, W. Solvent Free Synthesis of PdZn/TiO2 Catalysts for the Hydrogenation of CO2 to Methanol. *Top. Catal.* **2018**, *61* (3), 144−153.
(25) Zhou, C.; Xu, L.; Song, J.; Xing, R.; Xu, S.; Liu, D.; Song, H. Ultrasensitive non-enzymatic glucose sensor based on three-dimensional network of ZnO-CuO hierarchical nanocomposites by electrospinning. *Sci. Rep.* **2015**, *4*, 7382.
(26) Conant, T.; Karim, A. M.; Lebarbier, V.; Wang, Y.; Girgsdies, F.; Schlögl, R.; Datye, A. Stability of bimetallic Pd−Zn catalysts for the steam reforming of methanol. *J. Catal.* **2008**, *257* (1), 64−70.
(27) Karim, A.; Conant, T.; Datye, A. The role of PdZn alloy formation and particle size on the selectivity for steam reforming of methanol. *J. Catal.* **2006**, *243* (2), 420−427.
(28) Sun, J.; Yang, G.; Yoneyama, Y.; Tsubaki, N. Catalysis Chemistry of Dimethyl Ether Synthesis. *ACS Catal.* **2014**, *4* (10), 3346−3356.
(29) Gao, Y.; Zheng, B.; Wu, G.; Ma, F.; Liu, C. Effect of the Si/Al ratio on the performance of hierarchical ZSM-5 zeolites for methanol aromatization. *RSC Adv.* **2016**, *6* (87), 83581−83588.
(30) Zhang, Y.; Cai, Y.; Guo, Y.; Wang, H.; Wang, L.; Lou, Y.; Guo, Y.; Lu, G.; Wang, Y. The effects of the Pd chemical state on the activity of Pd/Al2O3 catalysts in CO oxidation. *Catal. Sci. Technol.* **2014**, *4* (11), 3973−3980.
(31) Cubeiro, M. L.; Fierro, J. L. G. Partial oxidation of methanol over supported palladium catalysts. *Appl. Catal., A* **1998**, *168* (2), 307−322.
(32) Dumbuya, K.; Denecke, R.; Steinrück, H. P. Surface analysis of Pd/ZnO catalysts dispersed on micro-channeled Al-foils by XPS. *Appl. Catal., A* **2008**, *348* (2), 209−213.
(33) Deroubaix, G.; Marcus, P. X-ray photoelectron spectroscopy analysis of copper and zinc oxides and sulphides. *Surf. Interface Anal.* **1992**, *18* (1), 39−46.
(34) Kuld, S.; Conradsen, C.; Moses, P. G.; Chorkendorff, I.; Sehested, J. Quantification of Zinc Atoms in a Surface Alloy on Copper in an Industrial-Type Methanol Synthesis Catalyst. *Angew. Chem., Int. Ed.* **2014**, *53* (23), 5941−5945.
(35) Hoang, D. L.; Dang, T. T. H.; Engeldinger, J.; Schneider, M.; Radnik, J.; Richter, M.; Martin, A. TPR investigations on the reducibility of Cu supported on Al2O3, zeolite Y and SAPO-5. *J. Solid State Chem.* **2011**, *184* (8), 1915−1923.
(36) Hunger, B.; Hoffmann, J.; Heitzsch, O.; Hunger, M. Temperature- programmed desorption (TPD) of ammonia from HZSM-5 zeolites. *J. Therm. Anal.* **1990**, *36* (4), 1379−1391.
(37) Iwasaki, M.; Yamazaki, K.; Banno, K.; Shinjoh, H. Characterization of Fe/ZSM-5 DeNOx catalysts prepared by different methods: Relationships between active Fe sites and NH3-SCR performance. *J. Catal.* **2008**, *260* (2), 205−216.
(38) Vorobyeva, N.; Rumyantseva, M.; Filatova, D.; Konstantinova, E.; Grishina, D.; Abakumov, A.; Turner, S.; Gaskov, A. Nanocrystalline ZnO(Ga): Paramagnetic centers, surface acidity and gas sensor properties. *Sens. Actuators, B* **2013**, *182*, 555−564.
(39) Shen, W.-J.; Jun, K.-W.; Choi, H.-S.; Lee, K.-W. Thermodynamic investigation of methanol and dimethyl ether synthesis from CO2 Hydrogenation. *Korean J. Chem. Eng.* **2000**, *17* (2), 210−216.
(40) Bahruji, H.; Bowker, M.; Brookes, C.; Davies, P. R.; Wawata, I. The adsorption and reaction of alcohols on TiO2 and Pd/TiO2 catalysts. *Appl. Catal., A* **2013**, *454*, 66−73.
(41) Ghorbanpour, A.; Rimer, J. D.; Grabow, L. C. Computational Assessment of the Dominant Factors Governing the Mechanism of Methanol Dehydration over H-ZSM-5 with Heterogeneous Aluminum Distribution. *ACS Catal.* **2016**, *6* (4), 2287−2298.
(42) Jones, A. J.; Iglesia, E. Kinetic, Spectroscopic, and Theoretical Assessment of Associative and Dissociative Methanol Dehydration Routes in Zeolites. *Angew. Chem., Int. Ed.* **2014**, *53* (45), 12177−12181.
(43) Li, J.; Wei, Y.; Liu, G.; Qi, Y.; Tian, P.; Li, B.; He, Y.; Liu, Z. Comparative study of MTO conversion over SAPO-34, H-ZSM-5 and H-ZSM-22: Correlating catalytic performance and reaction mechanism to zeolite topology. *Catal. Today* **2011**, *171* (1), 221−228.
(44) Hajimirzaee, S.; Ainte, M.; Soltani, B.; Behbahani, R. M.; Leeke, G. A.; Wood, J. Dehydration of methanol to light olefins upon zeolite/alumina catalysts: Effect of reaction conditions, catalyst support and zeolite modification. *Chem. Eng. Res. Des.* **2015**, *93*, 541−553.
(45) Akarmazyan, S. S.; Panagiotopoulou, P.; Kambolis, A.; Papadopoulou, C.; Kondarides, D. I. Methanol dehydration to dimethylether over Al2O3 catalysts. *Appl. Catal., B* **2014**, *145*, 136−148.
(46) Rownaghi, A. A.; Rezaei, F.; Stante, M.; Hedlund, J. Selective dehydration of methanol to dimethyl ether on ZSM-5 nanocrystals. *Appl. Catal., B* **2012**, *119−120* (Supplement C), 56−61.
(47) Bahruji, H.; Bowker, M.; Hutchings, G.; Dimitratos, N.; Wells, P.; Gibson, E.; Jones, W.; Brookes, C.; Morgan, D.; Lalev, G. Pd/ZnO catalysts for direct CO2 hydrogenation to methanol. *J. Catal.* **2016**, *343*, 133−146.

DOI: 10.1021/acs.iecr.8b00230
Ind. Eng. Chem. Res. 2018, 57, 6821−6829